Journal of Materials Chemistry A

Accepted Manuscript

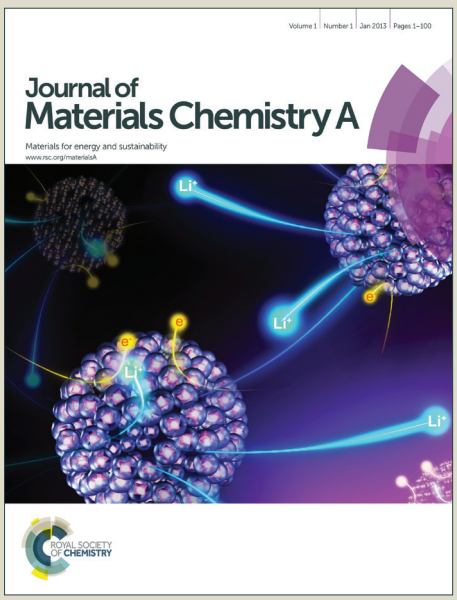

ROYAL SOCIETY OF CHEMISTRY

www.rsc.org/materialsA

Journal of Materials Chemistry A

RSC Publishing

ARTICLE

One-step synthesis of multi-walled carbon nanotubes/ ultra-thin $Ni(OH)_2$ nanoplate composite as efficient catalysts for water oxidation

Cite this: DOI: 10.1039/x0xx00000x

Received 00th January 2012,
Accepted 00th January 2012

DOI: 10.1039/x0xx00000x

www.rsc.org/

Xuemei Zhou,[a] Zhiyun Zhang, [a] Yuanyuan Ma,*[a,b] and Yongquan Qu*[a,b]

We report a novel approach to synthesize ultra-thin β-$Ni(OH)_2$ nanoplates with a thickness of 1.5 ~ 3.0 nm and their composite with multi-walled carbon nanotubes (MWCNTs) by one-step hydrothermal in the absence of surfactants. Ultra-thin β-$Ni(OH)_2$ nanoplates have a large surface area of 139.0 m^2/g associated with more exposed surface Ni species and exhibit better catalytic activity for oxygen evolution reaction (OER) than that of thick β-$Ni(OH)_2$ nanoplates previously reported. Compared to β-$Ni(OH)_2$ nanoplates alone and MWCNTs+ $Ni(OH)_2$ nanoplate physical mixture, the composite exhibits much higher electrocatalytic OER activity in terms of low onset overpotential, small Tafel slope, large exchange current density and high OER catalytic current densities at specific applied potentials. The Tafel slope of 87 mV/dec for the composite in pH 13 KOH is much smaller than that of β-$Ni(OH)_2$ nanoplates (165 mV/dec) and their physical mixture (140 mV/dec). The enhanced catalytic activity of the MWCNTs/$Ni(OH)_2$ composite could be described to the synergic interface of MWCNTs and ultra-thin β-$Ni(OH)_2$ nanoplates for improved conductivity, efficient chemical transfer and high oxidation state of Ni species in the composite electrodes by introducing MWCNTs. No obvious degradation of the OER catalytic current density of the composite electrode over a period of six hours was observed.

Introduction

Photo-assisted water splitting, representing a practical approach to convert solar energy into chemical energy, has attracted considerable interest.[1-8] Ideally, a semiconductor with a band gap $E_g > 1.23$ eV and the suitable energy levels of conduction band and valence band (E_{cb} and E_{vb}) that straddle the redox potentials of H^+/H_2O (0 V *vs.* NHE) and O_2/H_2O (1.23 V *vs.* NHE), can drive the hydrogen evolution reaction (HER) and oxygen evolution reaction (OER) under light irradiation.[1-4, 8] However, the required energy reported for the photoelectrolysis on a semiconductor is always above 1.8 eV due to energy loss at the interface of solid catalysts and liquid electrolyte and kinetic overpotential.[3, 8] The co-catalysts to facilitate the desired redox reactions are integrated to the semiconductor to lower the overpotentials for HER and OER.[9] OER involving a four-electron process is kinetically more difficult and challenging than HER, a two-electron process.[10] Although previous investigations indicate that Ir- and Ru- based catalysts show remarkable OER catalytic activities, their practical utilizations are limited by their rare availability and high cost.[11-13]

The intensive search for economical substitutes with high efficiency as OER catalysts is extremely expected. Besides, the stability of OER catalysts is another concern for the practical applications because the direct electrochemical reactions on the OER catalyst may cause the detrimention and degradation of the catalyst itself. Mimicking to the nature photosystem II in which $CaMn_4O_4$ works as the catalytic sites for O_2 generation, the oxides, hydroxides and oxy-hydroxides of the first raw transitional metals has been considered as the potential cost-effective OER catalysts to replace the precious catalysts.[6, 14-16] For example, NiOOH functioning as the dual roles of OER catalysts and protective layer can significantly improve the efficiency and stability of silicon photoanodes for photoelectrocatalytic water splitting.[17-20]

Compared to widely explored Co,[6, 21-23] Fe[23, 24] and Mn[23, 25, 26]-based OER catalysts, Ni species including NiO, $Ni(OH)_2$ and

NiOOH are less appealing as the OER catalysts due to their low efficiency and poor stability. Previous investigations of OER activity of Ni-based catalysts were mainly performed on electrodeposited or physical deposited thin film of nanostructured Ni species on the conductive supports.[18, 27-31] Thin thickness of catalytic layer and homogeneous contact between catalysts and conductive support ensure the efficient charge transportation within the catalytic electrode, leading to the high activity of Ni-based OER catalysts. In contrast, freestanding nanostructures of Ni-based OER catalysts have been seldom explored, which always exhibited high overpotentials at specific OER current densities and large Tafel slope.[32] It has been widely recognized that the nanostructured conductive supports such as multi-walled carbon nanotubes (MWCNTs)[33-38] and graphene[32, 39, 40] can greatly improve the electrocatalytic activity of catalysts. Recently, NiO_x/Ni naoparticles anchored on N-doped graphene 3D electrode showed high activity and excellent durability in alkaline environment.[32, 41] However, the achieved Tafel slope of the 3D electrode was 188.6 mV/dec,[32] which is much larger than that of NiO_x thin film (40 ~ 120 mV/dec)[27-29] prepared by electrodeposition. Importantly, the nanostructured OER catalysts loaded on the surface of semiconductors are required for photo-assisted water splitting, demonstrating the importance to study the catalytic behavior of freestanding Ni-based catalysts. Hence, seeking for optimized structures of Ni-based nanomaterials as efficient and stable OER catalysts is still desired.

β-$Ni(OH)_2$, with a well-defined layered structure (a= 3.12 Å and c=4.60 Å, Fig. 1a), is widely used as a catalyst in the electro-oxidation due to the easily formed redox pair β-$Ni(OH)_2$/β-NiOOH.[42-44] In this work, we report a novel hydrothermal approach to synthesize β-$Ni(OH)_2$ nanoplates with small size of 20 ~ 50 nm and ultra-thin thickness of 1.5 ~ 3.0 nm and their composite with MWCNTs as OER catalysts in the absence of surfactants. The β-$Ni(OH)_2$ nanoplates with their unique morphological features offer a large surface area (139.0 m^2/g) and suggest high fraction of surface Ni atom and exposed corner and edge Ni atoms with a low coordination number as the catalytic sites for OER. The composite is synthesized by introducing MWCNTs to afford the in-stiu growth of β-$Ni(OH)_2$ nanoplates and form interconnected electrically conducting networks for the OER catalytic electrodes. The framework created by MWCNTs and the interplay interface between MWCNTs and β-$Ni(OH)_2$ nanoplates of the composite ensure both efficient charge transport and fast chemical transfer for the OER electrodes. Compared to the MWCNTs+$Ni(OH)_2$ physical mixture and β-$Ni(OH)_2$ nanoplates alone, the MWCNTs/$Ni(OH)_2$ composite exhibits superior performances for OER including low Tafel slope (87 mV/dec), high TOF (0.052 s^{-1} for each Ni atom) at 0.85 V (*vs.* Ag/AgCl) and undegraded OER current density over six hours at 0.7 V (*vs.* Ag/AgCl) in aqueous alkaline electrolyte solution of pH 13.0.

Experimental

Surface treatment of MWCNTs

Pristine MWCNTs were purified by high temperature annealing at 500 °C for 10 min in a tube furnace in air to remove amorphous carbon. Then, the products were refluxed in concentrated HCl and HNO_3 (v/v = 3:1) mixed solution for 30 min at room temperature to remove residual metal components. The treated MWCNTs were filtered through a 0.45-μm filter, rinsed with deionized water until the pH of the filtered solution reached 7.0, and dried in an electric oven at 80 °C.

Preparation of ultra-thin β-$Ni(OH)_2$ nanoplates

β-$Ni(OH)_2$ nanoplates were prepared by hydrothermal. In a typical synthesis, NaOH (0.16 mol) was dissolved in 35 mL of Milli-Q water (18.2 MΩ · cm) under vigorous magnetic stirring at room temperature. $Ni(NO_3)_2 \cdot 6H_2O$ (2 mmol) dissolved in 5 mL MQ water was slowly injected into NaOH aqueous solution. After aging for 30 min under continuous stirring, the mixture was treated with hydrothermal at 100 °C. After 12 hr hydrothermal, the reaction was cooled down to room temperature naturally. The products were filtered, washed thoroughly with MQ water and absolute ethanol, and dried at 60 °C overnight.

Preparation of MWCNTs/β-$Ni(OH)_2$ composites

The MWCNTs/β-$Ni(OH)_2$ composites were synthesized by a facile one-step method. In a typical synthesis, 6.4 g NaOH was dissolved in 35 ml of MQ water under vigorous magnetic stirring at room temperature. MWCNTs and $Ni(NO_3)_2 \cdot 6H_2O$ dissolved in 5 ml MQ water were slowly added into NaOH aqueous solution. After aging for 30 min under continuous stirring, the mixture was transferred into a Pyrex bottle and placed into an electric oven. After hydrothermal at 100 °C for 12 h, the reaction was cooled down to room temperature naturally. The final products were filtered, washed thoroughly with MQ water and absolute ethanol, and dried at 60 °C overnight. The MWCNTs content in the composites was determined by thermal-gravimetric analysis, in which the composite material was heated in air with a ramping rate of 5 °C · min^{-1}.

Preparation of a physical mixture of MWCNTs and β-$Ni(OH)_2$

The physical mixture of MWCNTs and β-$Ni(OH)_2$ was prepared by sonicating the free β-$Ni(OH)_2$ nanoplates with certain amount of MWCNT in MQ water. The mixtures were then collected by centrifugation and dried at 80 °C. The products were denoted as MWCNTs+$Ni(OH)_2$ mixture.

Preparation of thick β-$Ni(OH)_2$ nanoplates

Thick β-$Ni(OH)_2$ nanoplates, named as $Ni(OH)_2$-R, were prepared according to previous method.[39] 0.2 mL of ammonia solution (28 wt.% in water) and 2 mL of 0.4 M $Ni(NO_3)_2$ aqueous solution were added successively into 10 mL MQ water. The mixture was subjected to sonication for 10 min and then sealed in a Teflon-lined autoclave and maintained at 180 °C for 2 h. The autoclave was naturally cooled to room temperature. The products were filtered, washed thoroughly with MQ water and absolute ethanol, and dried at 60 °C overnight.

Characterization of catalysts

The surface area and pore size were measured by nitrogen physisorption (Quantachrome, Autosorb-iQ) based on the Brunauer-Emmet- Teller (BET) method. The phase evolution of as-synthesized nanostructures was monitored by powder X-ray diffraction (XRD). The XRD patterns with diffraction intensity versus 2θ were recorded in a Shimadzu X-ray diffractometer (Model 6000) using Cu K_α radiation. Thermogravimetric analysis (TGA) of as-synthesized samples were carried out Mettler Toledo, STAR^e at a heating rate of 5 °C · min^{-1} from room temperature to 800 °C in air. X-ray photoelectron spectra (XPS) data was acquired on a Thermo Electron Model K-Alpha with Al K_α as the excitation source. Scanning electron microscopy (SEM) was performed on Hatchie Su-8010 scanning electron microscope. Transmission electron microscopy (TEM) studies were conducted on a Hatchie HT-7700 field-emission transmission electron microscope with an accelerating voltage of 120 kV.

Electrochemical measurements

Electrocatalytic activities including linear sweep voltammograms (LSV) and chronoamperometry were measured on CHI 660D electrochemistry workstation (CH Instrument, Shanghai, China) with a standard three electrode system in KOH aqueous solutions at various concentrations of 0.01 M, 0.1 M and 1.0 M. The counter electrode was platinum wire and the reference electrode was standard Ag/AgCl (3M KCl) electrode. The catalyst with a loading of 0.28 mg · cm^{-2} on indium tin oxide (ITO) surface was used as the working electrode. The scanning rate for LSV measurements was 50 mV · s^{-1}. The chronoamperometric response of samples was obtained at 0.7 V vs. Ag/AgCl in 0.1 M KOH aqueous solutions. Electrochemical impedance spectroscopy (EIS) was performed on the AUTOLAB PGSTAT204 electrochemistry workstation in the frequency range from 0.1 Hz to 100 KHz at an open circuit potential, with 10 mV as the amplitude potential.

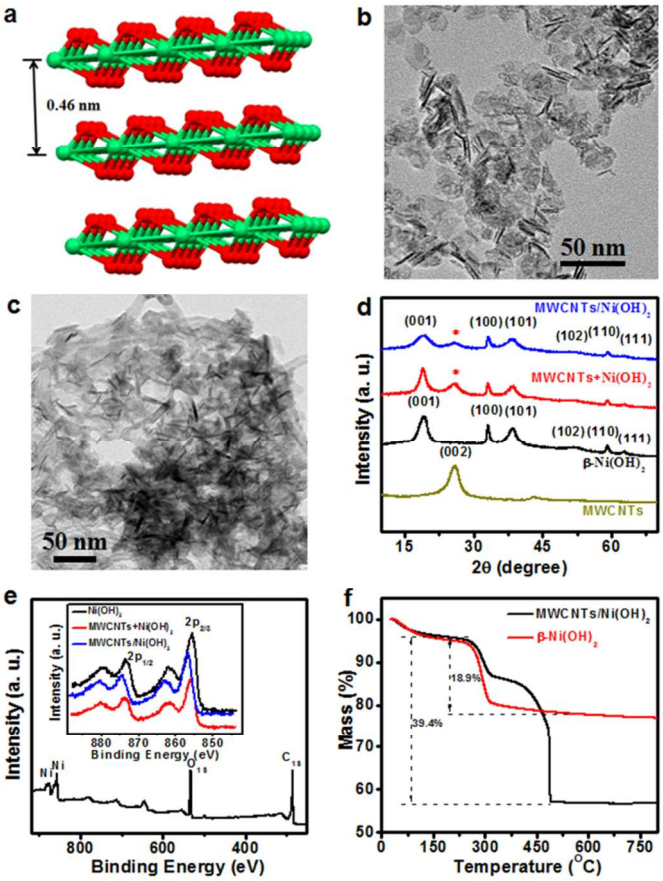

Fig. 1 Structure characterization of freestanding ultra-thin β-$Ni(OH)_2$ nanoplates and MWCNTs/$Ni(OH)_2$ composite. (a) Layered structures of β-$Ni(OH)_2$. Green and red balls represent the Ni and O, respectively. (b) Typical TEM image of ultra-thin β-$Ni(OH)_2$ nanoplates. (c) Typical TEM image of MWCNTs/$Ni(OH)_2$ composite. (d) XRD spectra of β-$Ni(OH)_2$ nanoplates, MWCNTs, MWCNTs/$Ni(OH)_2$ composite and MWCNTs+$Ni(OH)_2$ mixture. (e) XPS survey spectrum of MWCNTs/$Ni(OH)_2$ composite. The inset is Ni 2p spectra of ultra-thin β-$Ni(OH)_2$, MWCNTs/$Ni(OH)_2$ composite and MWCNTs+$Ni(OH)_2$ mixture. (f) TGA curve for ultra-thin β-$Ni(OH)_2$ nanoplates and MWCNTs/$Ni(OH)_2$ composite in air with a temperature ramp rate of 5 °C/min.

Results and Discussion

Ultra-thin β-$Ni(OH)_2$ nanoplates were synthesized by a modified method previously reported,[45-47] in which the aqueous mixture of $Ni(NO_3)_2{\cdot}6H_2O$ and NaOH were aged at 100 °C for 12 h. The synthesis is carried out in the absence of surfactants and effectively avoids the possible contamination from surfactants to the catalytic sites of Ni-based catalysts. TEM image (Fig. 1b) shows that the size of near hexagonal $Ni(OH)_2$ nanoplates is about 20 ~ 50 nm and nearly transparent to electron beam indicates the ultra-thin nature. From the vertically aligned nanoplates shown in Fig. 1a, the thickness of the $Ni(OH)_2$ nanoplates is 1.5 ~ 3.0 nm. To our knowledge, our synthesis is the first example to synthesize such thin freestanding $Ni(OH)_2$ nanoplates without assistant of surfactants in aqueous phase. MWCNTs/$Ni(OH)_2$ composite was synthesized by a similar one-step synthetic approach of freestanding $Ni(OH)_2$ nanoplates, except MWCNTs was added during synthesis. The microstructure and texture of as-synthesized composite were examined with a series of characterizations. Typical TEM image (Fig. 1c) clearly demonstrates the nanoplates successfully grown on MWCNTs. The nanoplates preserve the features of small size and ultra-thin thickness as similar as to that of the freestanding nanoplates. Of note, the morphology of nanoplates in the composite is more irregular than those prepared in the absence of MWCNTs (Fig. 1c), indicating the MWCNTs influenced the growth of $Ni(OH)_2$. Such phenomena were also observed in the composites of nickel oxides and hydroxides with carbon nanomaterials.[39, 48, 49]

Fig. 1d reveals the XRD patterns of $Ni(OH)_2$ nanoplates, MWCNTs and their composite and physical mixture. XRD spectrum clearly indicates β-$Ni(OH)_2$ phase (JCPDS No. 14-0117). Compared to the freestanding $Ni(OH)_2$ nanoplates, both the composite and the physical mixture show the characteristic diffraction peaks of β-$Ni(OH)_2$ and no peaks for Ni and NiO, indicating the formation of pure β-$Ni(OH)_2$ in the composite

and physical mixture. A predominant diffraction peak around 26 ° belongs to the characteristic (002) reflection of the layered graphite structure, indicating the presence of MWCNTs in the composite and physical mixture.

XPS measurements were also employed to analyze the chemical states of all elements in the β-$Ni(OH)_2$ nanoplates, MWCNTs/$Ni(OH)_2$ composite and MWCNTs+$Ni(OH)_2$ mixture. The presence of Ni, O and C in the composite is confirmed by the survey XPS spectrum of MWCNTs/$Ni(OH)_2$ composite (Fig. 1e). Compared with the XPS characteristic peak at 855.4 eV assigned to Ni 2p of pure β-$Ni(OH)_2$ nanoplates, the slight shift of this Ni 2p peak of the composite to 856.7eV (Fig. 1e inset) can probably be attributed to the interactions between β-$Ni(OH)_2$ and MWCNTs, which has been observed in the previous reports on the conjugation of metal oxides or hydroxides with carbon materials.[34, 35] To verify this phenomenon, a controlled XPS experiment on the MWCNTs+$Ni(OH)_2$ physical mixture was also performed. As shown in Fig. 1d, unshifted Ni 2p peak at 855.4 eV for the physical mixture further confirmed such a shift in the composite was induced by the hybrid interaction between MWCNTs and $Ni(OH)_2$. The XPS spectra indicated the successful growth of β-$Ni(OH)_2$ nanoplates on MWCNTs and formation of the composite.

The MWCNTs content in the composite was determined by TGA (Fig. 1f). In the TGA curve of β-$Ni(OH)_2$ nanoplates, a sharp weight loss of 18.9% around 300 °C is corresponded to the dehydration of $Ni(OH)_2$ into NiO with a theoretical weight loss of 19.4%. As temperature raised, two sharp weight loss peaks of the MWCNTs/$Ni(OH)_2$ composite were observed around 300 °C and 460 °C, which could be attributed to the dehydration of $Ni(OH)_2$ and combustion of MWCNTs. The total weight loss for the composite was 39.4%, as observed from the TGA curve. The calculated weight ratio of MWCNTs in the composite was 27%, which was used to prepare the physical mixture of MWCNTs and β-$Ni(OH)_2$ nanoplates.

To evaluate the OER activities of the catalysts, the MWCNTs/$Ni(OH)_2$ composite, MWCNTs+$Ni(OH)_2$ mixture and β-$Ni(OH)_2$ nanoplates were loaded onto an indium-tin oxide (ITO) electrode by drop casting method with a density of 0.28 mg/cm^2 for the electroactive Ni species. The thermodynamic potentials for the electrodes, $E^o_{OH^-/O2}$ = 0.324 V *vs.* Ag/AgCl at pH=12, 0.265 V *vs.* Ag/AgCl at pH=13, and 0.206 V *vs.* Ag/AgCl at pH=14, were used for all overpotential measurements in different concentrations of KOH electrolyte solutions in a standard three-electrode cell.[50, 51] Undistorted iR- corrected polarization curves of the MWCNTs/$Ni(OH)_2$ composite on ITO electrodes in pH 13.0 KOH (Fig. S1, ESI †) indicate that 95% iR compensation is an optimal compensation level for the catalysts.

The anodic current curves of the MWCNTs/$Ni(OH)_2$ composite, MWCNTs+$Ni(OH)_2$ mixture, β-$Ni(OH)_2$ nanoplates and MWCNTs electrodes in pH 13.0 KOH electrolyte solution are shown in Fig. 2a. As expected, the near zero current density of ITO substrate itself over the whole window of applied potentials indicates the inactive nature of bare ITO towards O_2 evolution. A sharp onset OER current for MWCNTs/$Ni(OH)_2$

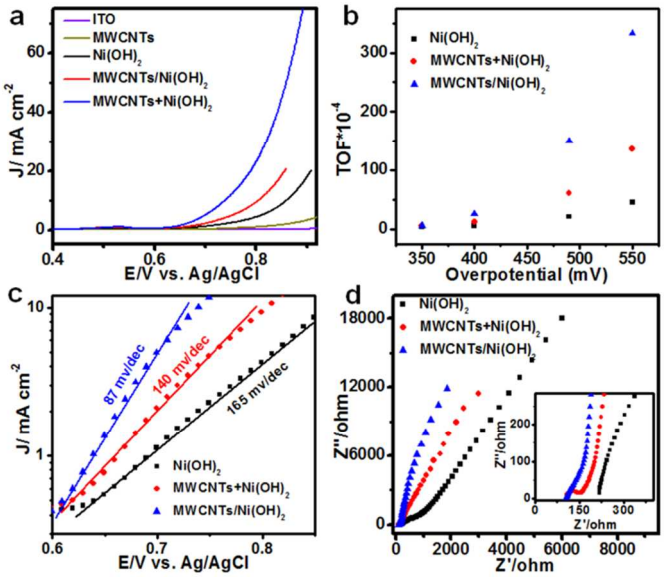

Fig. 2 Electrochemical performance of freestanding ultra-thin β-$Ni(OH)_2$ nanoplates (black), MWCNTs (dark yellow), MWCNTs/$Ni(OH)_2$ composite (blue) and MWCNTs+$Ni(OH)_2$ physical mixture (red) loaded on ITO electrodes. (a) Linear sweep voltammograms of all catalytic electrodes in pH 13.0 KOH with 95% iR corrections. The scanning rate was 50 mV/min. (b) The derived TOF values of three catalysts at different overpotentials in pH 13.0 KOH electrolyte, assuming all Ni atoms are active sites. (c) Tafel plots of three catalysts loaded on ITO recorded in pH=13 KOH, corresponding to the LSV curves in Fig. 2a. (d) Impedance Nyquist plots of three catalysts in pH 13.0 KOH electrolyte solution.

composite at 0.60 V versus Ag/AgCl electrode was observed. In contrast, MWCNTs+$Ni(OH)_2$ mixture and β-$Ni(OH)_2$ nanoplate electrodes displayed the similar onset potentials, which were 15 mV and 28 mV larger than that of the MWCNTs/$Ni(OH)_2$ composite, respectively.

The electrocatalytic activities of all catalysts in pH 13.0 KOH including the overpotentials at a specified current density (1 or 5 or 10 or 20 mA/cm^2), the current densities at 0.85 V (vs. Ag/AgCl) and turnover frequency (TOF), are summarized in Table 1. As presented in Fig. 2a, the current density of the MWCNTs/$Ni(OH)_2$ composite was definitely higher than that of other catalysts over the whole potential range. The current density of MWCNTs/$Ni(OH)_2$ composite at 0.85 V (vs. Ag/AgCl) was 44.37 mA/cm^2, which was 2.4 and 5.1 times higher than those of MWCNTs+$Ni(OH)_2$ mixture (18.45 mA/cm^2) and β-$Ni(OH)_2$ nanoplates (8.71 mA/cm^2), respectively. The results indicate that the MWCNTs/$Ni(OH)_2$ composite is a highly active OER catalyst. The amount of generated O_2 for the composite electrodes was also confirmed by a Benchtop DO Meter (Thermo Scientific Orion Star A213). As shown in Fig. S2 (ESI †), 1.5 μmol O_2 was generated within 1 hour for a composite electrode at 0.8 V (vs. Ag/AgCl). Compared to the theoretical value, the Columbia efficiency for the composite electrodes is ~ 90%.

The turnover frequency (TOF) for each catalyst can be calculated from the electrode current density at a specific overpotential, assuming Faraday efficiency is 100 % and every nickel atom is an active site for OER. As shown in Fig. 2b, the MWCNTs/$Ni(OH)_2$ composite, MWCNTs+$Ni(OH)_2$ mixture and β-$Ni(OH)_2$ nanoplates

Table1. Summary of the samples for their OER electrocatalytic activities in pH=13 KOH.

	η onset (mV)	η (mV) $^{-2}$ 1 mA cm	η (mV) $^{-2}$ 5 mA cm	η (mV) $^{-2}$ 10 mA cm	η (mV) $^{-2}$ 20 mA cm	J (mA cm $^{-2}$) @0.85V	TOF×10 $^{-2}$ (η=490 mV)	j_o (μA cm $^{-2}$)	BET (m^2 g)
$Ni(OH)_2$	350	427	546	595	643	8.71	0.21	0.14	139.0
MWCNTs +$Ni(OH)_2$	337	398	489	540	592	18.45	0.61	0.45	147.4
MWCNTs /$Ni(OH)_2$	322	373	435	474	524	44.37	1.50	2.0	161.9

j_o: Exchange current density

achieved TOFs 2.57 × 10^{-3}, 1.24 × 10^{-3} and 5.70 × 10^{-4} s^{-1}, respectively, in pH 13.0 KOH electrolyte solution at the overpotential of 400 mV, indicating that the highest activity was observed for the electrode loaded with MWCNTs/$Ni(OH)_2$ composite catalysts. At an OER current density of 1.0 mA/cm^2, the MWCNTs/$Ni(OH)_2$ composite demonstrates a smaller overpotential of 373 mV than those of MWCNTs/$Ni(OH)_2$ mixture (398 mV) and β-$Ni(OH)_2$ nanoplates (427 mV). Similar tendency is also observed at other specific OER current densities, as summarized in Table 1. Increasing the OER current density, the required overpotentials for catalysts were also increased for all catalysts (Table 1). The highest TOFs at a specific overpotential and the lowest overpotentials at a specific current density of the composite electrodes (Fig. 2 and Table 1) further illustrate the highest OER activity of the MWCNTs/$Ni(OH)_2$ composite. Although it is difficult to directly compare the TOFs of our Ni-based electrocatalysts with previously reported ones due to the differences in catalyst synthesis methods, catalysts loading, types of supports, pH value of electrolyte solution, *et.al*,[51] the TOFs of the MWCNTs/$Ni(OH)_2$ composite exhibit higher values than those of previously reported Ni-based OER catalysts. NiO_x-en thin film deposited from molecular precursor showed a TOF of 0.015 s^{-1} at 1.10 V (*vs.* Ag/AgCl) applied potential.[31] In contrast, a larger TOF of 0.053 s^{-1} at 0.85 V (*vs.* Ag/AgCl) for the composite electrode was obtained.

We also fitted the polarization curves of MWCNTs/$Ni(OH)_2$ composite, MWCNTs+$Ni(OH)_2$ mixture and β-$Ni(OH)_2$ nanoplates (Fig. 2a) to the Tafel equation $\eta = b\ log(j/j_0)$,[33] where η is the overpotential, b is the Tafel slope, j is the current density and j_0 is the exchange current density. As presented in Fig. 2c, the derived Tafel slope of 87 mV/dec for MWCNTs/$Ni(OH)_2$ composite is much smaller than those for MWCNTs+$Ni(OH)_2$ mixture (140 mV/dec) and β-$Ni(OH)_2$ (165 mV/dec) and in the range (40 - 120 mV/dec) reported for freshly electrodeposited NiO_x thin film on conductive substrate.[27-29] The value of Tafel slope of MWCNTs/$Ni(OH)_2$ composite is significantly decreased, compared to those that reported for Ni@NiO nanoparticle/N-doped graphene composite (188.6 mV/dec)[32] and NiO_x electrodeposited from nickel molecular complexes (104 mV/dec),[31] suggesting a high OER activity of the MWCNTs/$Ni(OH)_2$ composite. By applying extrapolation method to the Tafel plots, the calculated exchange current densities j_0 are obtained (Fig. S3, ESI † and Table 1). As shown in Table 1, the j_0 of MWCNTs/$Ni(OH)_2$ composite is 2.0 μA/cm^2, which is 4.44 times larger than that of MWCNTs+$Ni(OH)_2$ mixture and 14.3 times higher than the value of β-$Ni(OH)_2$ nanoplates, indicating faster and more favorable charge transfer at the MWCNTs/$Ni(OH)_2$ composite electrode.[52] Similar behavior was also observed in pH 14 KOH electrolyte solutions (Fig. S3 and Table S1, ESI †).

Current synthetic approach presents the structural features of as-synthesized β-$Ni(OH)_2$ nanoplates with the ultra-thin thickness (1.5 ~3.0 nm) and small size in range of 20 ~ 50 nm, as shown in Fig. 1a and 1b. In order to demonstrate the benefits of their structural features for OER, hexagonal β-$Ni(OH)_2$ nanoplates ($Ni(OH)_2$-R) with a thickness of 20 ~ 30 nm and side length of 60 ~ 100 nm (Fig. S4, ESI †) were prepared[39] and their OER catalytic activity was evaluated as a comparison. At low applied potentials, both ultra-thin β-$Ni(OH)_2$ nanoplates and $Ni(OH)_2$-R show similar OER catalytic activity in pH 13.0 KOH (Fig. S4c, ESI †). Increasing applied potentials, the OER current density for $Ni(OH)_2$-R falls behind that of our β-$Ni(OH)_2$ nanoplates. The current density of 17.9 mA/cm^2 at 0.9 V (vs. Ag/AgCl) for β-$Ni(OH)_2$ nanoplates is 2.2 times higher than 8.1 mA/cm^2 for $Ni(OH)_2$-R at same applied voltage. The derived Tafel slope (Fig. 3d) of $Ni(OH)_2$-R of 264 mV/dec is much larger than that of β-$Ni(OH)_2$ nanoplates (165 mV/dec).

The high activity of our Ni-based OER catalysts could be attributed to its unique morphology of ultra-thin β-$Ni(OH)_2$ nanoplate. First of all, small size of ultra-thin β-$Ni(OH)_2$ nanoplate can provide more surface area associated with more catalytic active sites for OER, as referred to their measured BET surface areas of 139.0 and 19.9 m^2/g for β-$Ni(OH)_2$ nanoplate and $Ni(OH)_2$-R, respectively. Secondly, the feature of the ultra-thin and small β-$Ni(OH)_2$ nanoplates also supplies higher amount of the corner and edge Ni species with a low coordination number. It is well known that the catalytic active sites with a low coordination number always display a higher activity, especially for the nanoscale catalysts. Assuming the β-$Ni(OH)_2$ nanoplates with a thickness of 2.5 nm and a side length of 30 nm, the calculated surface and corner/edge Ni percentages are 37.8% and 0.79%, which are much larger than the corresponded percentages of 3.74% and 0.032% for $Ni(OH)_2$-R with 25 nm thickness and 80 nm side length. Hence, high activity of ultra-thin β-$Ni(OH)_2$ nanoplates is expected and observed.

As summarized in Fig. 2 and Table 1, the MWCNTs/$Ni(OH)_2$ composite exhibits the highest OER activity compared to the physical mixture and β-$Ni(OH)_2$ nanoplates. The origin of the electrocatalytic enhancement for the composite electrode also could be attributed to the introduced MWCNTs with multiple functions during in stiu synthesis, forming a synergistic interplay at the interfaces of MWCNTs and β-$Ni(OH)_2$ nanoplates. First of all, combination of MWCNTs with β-

$Ni(OH)_2$ nanoplates can improve the conductivity of the catalytic electrode and hence benefit the charge transport. Especially, the hybrid interface of the MWCNTs/$Ni(OH)_2$ composite can significantly improve the charge transfer. Although the low conductivity of β-$Ni(OH)_2$, the morphological features of the ultra-thin and small β-$Ni(OH)_2$ nanoplates in the composite may benefit charge transfer as a shorter pathway for charge carrier transport. The detailed characteristics of the electrodes can be investigated with the electrochemical impedance spectroscopy (EIS). Typical Nyquist plots for the MWCNTs/$Ni(OH)_2$ composite, MWCNTs+$Ni(OH)_2$ mixture and β-$Ni(OH)_2$ nanoplates are presented in Fig. 2d. Compared to electrode resistances of the mixture (113 Ω) and β-$Ni(OH)_2$ nanoplates (172 Ω), the lowest electrode resistance of the composite (103 Ω) indicates the highest conductivity and the most efficient charge transport.

The composite electrode was also characterized by SEM. As shown in Fig. S5 (ESI †), the randomly distributed MWCNTs in the composite electrode create a framework with a large surface area and many large voids, which allow an easy access of the electrolyte to reach the catalytic sites, facilitate the chemical transfer within the MWCNTs/$Ni(OH)_2$ composite electrodes, and hence enhance the activity of the composite. Generally, the straight line in the low frequency of the Nyquist plots corresponds to the Warburg resistance relative to the diffusion of the electrolyte within the active electrode. The larger slope indicates the more efficient chemical transfer within the electrode. As evidenced in EIS spectra (Fig. 2d), the MWCNTs/$Ni(OH)_2$ composite exhibited the largest value of slope, indicating the high OER activity of the composite electrode.

It is generally accepted that β-$Ni(OH)_2$ can be oxidized to β-NiOOH in the aqueous alkaline media, which has been considered as the favorable Ni species for electrocatalytic OER. The mechanism for OER on Ni-based catalysts is expressed as:

$$OH^- \rightarrow (OH)_{ads} + e^- \quad (1)$$

$$(OH)_{ads} + OH^- \rightarrow (O^-)_{ads} + H_2O \quad (2)$$

$$2\beta\text{-NiOOH} + (O^-)_{ads} \rightarrow 2NiO_2 + H_2O + e^- \quad (3)$$

$$NiO_2 + (OH)_{ads} \rightarrow \beta\text{-NiOOH} + (O)_{ads} \quad (4)$$

$$2\,(O)_{ads} \rightarrow O_2 \quad (5)$$

The mechanism delivers the information that β-NiOOH is the right type of oxide providing the catalytic sites for OER.[32, 52] Starting from this understanding, further evidence of the high OER activity of the MWCNTs/$Ni(OH)_2$ composite is also revealed by their XPS spectra (Fig. 1e). Compared to the XPS Ni 2p spectra of three Ni-based catalysts, the shift to high energy of Ni 2p peaks of the composite indicates the lower electron density of the Ni atoms in the MWCNTs/$Ni(OH)_2$ composite. Hence, the higher oxidation state of Ni species in the composite than that in the physical mixture favors the formation of the β-NiOOH and in turn enhance the OER activity of the composite. This also could be used to explain the relative smaller onset potential of the MWCNTs/$Ni(OH)_2$ composite for OER. Besides, Ni-O-C may act as the alternative active centers to capture and oxidize OH^- into peroxide in alkaline electrolyte, which is decomposed to release O_2 gas in sequence.[32] The more positive charged Ni species in the composite have stronger ability to absorb OH^- for O_2 generation, compared to that of the physical mixture.

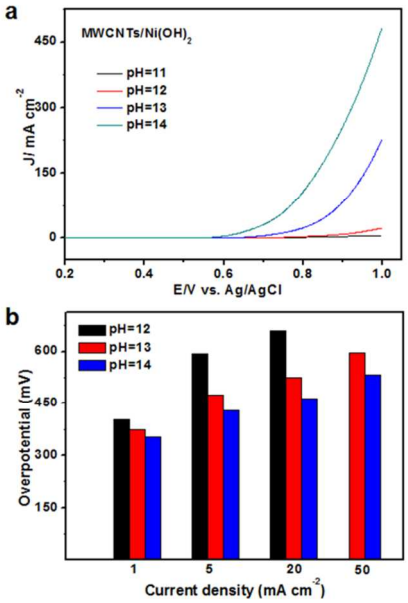

Fig. 3 (a) Linear voltammograms of the MWCNTs/$Ni(OH)_2$ composite electrodes in KOH electrolyte solutions with various pH values with 95% iR corrections. (b) Plot of overpotentials of the MWCNTs/$Ni(OH)_2$ composite *vs.* specific current densities of 1, 5, 20, 50 mA/cm^2 in pH 12, pH 13 and pH 14 KOH. In pH 12 KOH, the current densitity of 50 mA/cm^2 for the MWCNTs/$Ni(OH)_2$ composite electrode was not observed under the applied potentials of 0.2-1.0 V (vs. Ag/AgCl).

To further investigate the advantages of the MWCNTs/$Ni(OH)_2$ composite for OER, the catalytic activity of the catalysts was also evaluated in KOH electrolyte solutionswith various pH values of 11.0, 12.0 and 14.0. As shown in Fig. S6 (ESI †), the catalytic performance of four catalysts in different concentrations of KOH was very similar to that in pH 13.0 KOH media, in which MWCNTs/$Ni(OH)_2$ composite electrode showed the highest OER activities over the whole applied potential range. Plots of electrocatalytic activities of MWCNTs/$Ni(OH)_2$ composite *vs.* potential in various concentrations of KOH are given in Fig. 3a. A low current density of 2.31 mA/cm^2 at 0.85 V (*vs.* Ag/AgCl) was observed in pH=11 KOH solution. Increasing the concentration of KOH gives a much higher current density of 5.10, 44.37 and 172.82 mA/cm^2 at same applied potential for pH 12.0, 13.0 and 14.0 electrolyte solutions, respectively. As shown in Fig. 3b, the lower overpotentials of the composite electrodes were recorded at a specific OER current density for KOH electrolyte solution with higher pH values. The observations are very consistent with proposed mechanism (equation 1-5) and previous reports that raising the concentration of OH^- in the electrolyte can increase the OER activity of the first raw transitional metal based catalysts.[32, 50, 51]

Long-term durability of the catalysts towards OER is significant for future application in the area of energy generation/storage. The stability of the MWCNTs/$Ni(OH)_2$

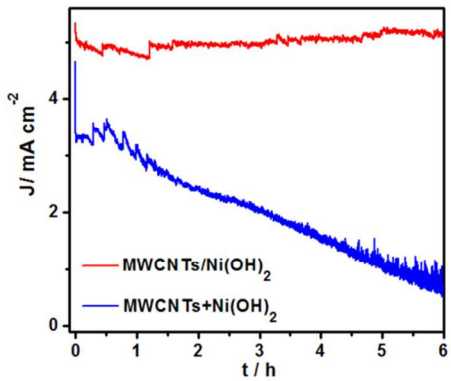

Fig. 4 Chronoamperometric measurements of the MWCNTs/Ni(OH)$_2$ composite and physical mixture biased at 0.7 V (*vs.* Ag/AgCl) in pH 13.0 KOH electrolyte solution.

composite and MWCNTs+Ni(OH)$_2$ mixture by running chronoamperometric responses (i-t) at 0.7 V (*vs.* Ag/AgCl) in pH 13.0 KOH aqueous solution was performed. As shown in Fig. 4, there was no obvious attenuation of MWCNTs/Ni(OH)$_2$ composite electrode during six hours. In contrast, a sharp activity loss of MWCNTs+Ni(OH)$_2$ physical mixture was observed at the initial period. After 4 hour running, only 42% of catalytic OER current density for the physical mixture electrode was preserved. The results indicates that MWCNTs/Ni(OH)$_2$ composite is a promising OER catalyst with high activity and strong durability.

Conclusions

In summary, a simple and cost-effective approach has been employed to synthesize ultra-thin β-Ni(OH)$_2$ nanoplates (1.5 ~ 3.0 nm) and in situ grow them onto conducting MWCNTs framework, which show drastic improvement in the electrochemical performance for water oxidation. The thin feature of the β-Ni(OH)$_2$ nanoplates in the composite supplies more catalytic active sites and facilitates charge transfer of the composite electrodes. The MWCNTs contribute to enhanced catalytic OER activity of Ni(OH)$_2$ by improving the electrical conductivity and creating voids for efficient chemical transfer. The synergistic interface of the MWCNTs/Ni(OH)$_2$ composite induces more positive charged surface Ni species, which facilitate the formation of catalytic active oxide of β-NiOOH and alternative Ni-O-C catalytic sites for OER. Combining with its excellent electrochemical stability, the MWCNTs/Ni(OH)$_2$ composite hold promise as a cost-effective OER catalyst.

Acknowledgements

We acknowledge the financial support from a NSFC Grant 21201138. This work was also partially funded by the Ministry of Science and Technology of China through a 973-program under Grant 2012CB619401 and the Fundamental Research Funds for the Central Universities. Technical supports for TEM experiments from TEM Laboratory of Frontier Institute of Science and Technology and SEM experiments from State Key Laboratory for Manufacturing Systems Engineering, Xi'an Jiaotong University, are also acknowledged.

Notes and references

[a]*Center of Applied Chemical Research, Frontier Institute of Science and Technology, Xi'an Jiaotong University, Xi'an, China 740049. E-mail: yongquan@mail.xjtu.edu.cn, yyma@mail.xjtu.edu.cn.*
[b]*Institute of Chemistry for New Energy Materials, Department of Chemistry, Xi'an Jiaotong University, Xi'an, China 740049.*

† Footnotes should appear here. These might include comments relevant to but not central to the matter under discussion, limited experimental and spectral data, and crystallographic data. Electronic Supplementary Information (ESI) available: [More characterizations of catalysts; calculations of j_o and TOF]. See DOI: 10.1039/b000000x/

1. M. W. Kanan, Y. Surendranath and D. G. Nocera, *Chem. Soc. Rev.*, 2009, **38**, 109-114.
2. D. G. Nocera, *Acc. Chem. Res.*, 2012, **45**, 767-776.
3. Y. Q. Qu and X. F. Duan, *Chem. Soc. Rev.*, 2013, **42**, 2568-2580.
4. Y. Q. Qu and X. F. Duan, *J. Mater. Chem.*, 2012, **22**, 16171-16181.
5. J. Barber, *Chem. Soc. Rev.*, 2009, **38**, 185-196.
6. F. Jiao and H. Frei, *Energy Environ. Sci.*, 2010, **3**, 1018-1027.
7. H. L. Zhou, Y. Q. Qu, T. Zeid and X. F. Duan, *Energy Environ. Sci.*, 2012, **5**, 6732-6743.
8. M. G. Walter, E. L. Warren, J. R. McKone, S. W. Boettcher, Q. X. Mi, E. A. Santori and N. S. Lewis, *Chem. Rev.*, 2010, **110**, 6446-6471.
9. S. Yusuf and F. Jiao, *Acs Catal.*, 2012, **2**, 2753-2760.
10. Y. Liang, Y. Li, H. Wang and H. Dai, *J. Am. Chem. Soc.*, 2013, **135**, 2013-2036.
11. G. Beni, L. M. Schiavone, J. L. Shay, W. C. Dautremont and B. S. Schneider, *Nature*, 1979, **282**, 281-283.
12. S. W. Gersten, G. J. Samuels and T. J. Meyer, *J. Am. Chem. Soc.*, 1982, **104**, 4029-4030.
13. H. Over, *Chem. Rev.*, 2012, **112**, 3356-3426.
14. F. Jiao and H. Frei, *Angew. Chem. Int. Ed.*, 2009, **48**, 1841-1844.
15. K. N. Ferreira, T. M. Iverson, K. Maghlaoui, J. Barber and S. Iwata, *Science*, 2004, **303**, 1831-1838.
16. G. P. Gardner, Y. B. Go, D. M. Robinson, P. F. Smith, J. Hadermann, A. Abakumov, M. Greenblatt and G. C. Dismukes, *Angew. Chem. Int. Ed.*, 2012, **51**, 1616-1619.
17. M. J. Kenney, M. Gong, Y. G. Li, J. Z. Wu, J. Feng, M. Lanza and H. J. Dai, *Science*, 2013, **342**, 836-840.
18. L. Trotochaud, J. K. Ranney, K. N. Williams and S. W. Boettcher, *J. Am. Chem. Soc.*, 2012, **134**, 17253-17261.
19. F. Lin and S. W. Boettcher, *Nat. Mater.*, 2014, **13**, 81-86.
20. K. Sun, X. L. Pang, S. H. Shen, X. Q. Qian, J. S. Cheung and D. L. Wang, *Nano Lett.*, 2013, **13**, 2064-2072.
21. C. A. Kent, J. J. Concepcion, C. J. Dares, D. A. Torelli, A. J. Rieth, A. S. Miller, P. G. Hoertz and T. J. Meyer, *J. Am. Chem. Soc.*, 2013, **135**, 8432-8435.
22. J. Rosen, G. S. Hutchings and F. Jiao, *J. Am. Chem. Soc.*, 2013, **135**, 4516-4521.
23. R. Subbaraman, D. Tripkovic, K. C. Chang, D. Strmcnik, A. P. Paulikas, P. Hirunsit, M. Chan, J. Greeley, V. Stamenkovic and N. M. Markovic, *Nat. Mater.*, 2012, **11**, 550-557.
24. N. T. Hahn, H. Ye, D. W. Flaherty, A. J. Bard and C. B. Mullins, *ACS Nano*, 2010, **4**, 1977-1986.
25. T. Takashima, K. Hashimoto and R. Nakamura, *J. Am. Chem. Soc.*, 2012, **134**, 18153-18156.
26. Y. Gorlin, B. Lassalle-Kaiser, J. D. Benck, S. Gul, S. M. Webb, V. K. Yachandra, J. Yano and T. F. Jaramillo, *J. Am. Chem. Soc.*, 2013, **135**, 8525-8534.
27. C. C. McCrory, S. Jung, J. C. Peters and T. F. Jaramillo, *J. Am. Chem. Soc.*, 2013, **135**, 16977-16987.
28. M. W. Louie and A. T. Bell, *J. Am. Chem. Soc.*, 2013, **135**, 12329-12337.
29. R. D. Smith, M. S. Prevot, R. D. Fagan, Z. Zhang, P. A. Sedach, M. K. Siu, S. Trudel and C. P. Berlinguette, *Science*, 2013, **340**, 60-63.
30. R. D. L. Smith, M. S. Prevot, R. D. Fagan, S. Trudel and C. P. Berlinguette, *J. Am. Chem. Soc.*, 2013, **135**, 11580-11586.

31. A. Singh, S. L. Y. Chang, R. K. Hocking, U. Bach and L. Spiccia, *Energy Environ. Sci.*, 2013, **6**, 579-586.
32. S. Chen, J. J. Duan, J. R. Ran, M. Jaroniec and S. Z. Qiao, *Energy Environ. Sci.*, 2013, **6**, 3693-3699.
33. M. Gong, Y. G. Li, H. L. Wang, Y. Y. Liang, J. Z. Wu, J. G. Zhou, J. Wang, T. Regier, F. Wei and H. J. Dai, *J. Am. Chem. Soc.*, 2013, **135**, 8452-8455.
34. Z. Yang, X. M. Zhou, H. G. Nie, Z. Yao and S. M. Huang, *ACS Appl. Mater. Interfaces*, 2011, **3**, 2601-2606.
35. J. Wu, Y. Xue, X. Yan, W. S. Yan, Q. M. Cheng and Y. Xie, *Nano Res.*, 2012, **5**, 521-530.
36. Z. Yang, X. M. Zhou, Z. P. Jin, Z. Liu, H. G. Nie, X. A. Chen and S. M. Huang, *Adv. Mater.*, 2014, DOI: 10.1002/adma.201305513.
37. X. M. Zhou, Z. M. Tian, J. Li, H. Ruan, Y. Y. Ma, Z. Yang and Y. Q. Qu, *Nanoscale*, 2014, **6**, 2603-2607.
38. L. T. Qu and L. M. Dai, *J. Am. Chem. Soc.*, 2005, **127**, 10806-10807.
39. Y. X. Xu, X. Q. Huang, Z. Y. Lin, X. Zhong, Y. Huang and X. F. Duan, *Nano Res.*, 2012, **6**, 65-76.
40. Y. Li, Y. Zhao, H. H. Cheng, Y. Hu, G. Q. Shi, L. M. Dai and L. T. Qu, *J. Am. Chem. Soc.*, 2012, **134**, 15-18.
41. S. Chen, J. J. Duan, M. Jaroniec and S. Z. Qiao, *Adv. Mater.*, 2014.
42. H. B. Liu, L. Xiang and Y. Jin, *Cryst. Growth Des.*, 2006, **6**, 283-286.
43. M. Shahid, J. J. Liu, I. Shakir, M. F. Warsi, M.Nadeem and Y. U. Kwon, *Electrochim. Acta*, 2012, **85**, 243-247.
44. S. M. Zhang and H. C. Zeng, *Chem. Mater.*, 2009, **21**, 871-883.
45. J. B. Wu, H. Zhang, N. Du, X. Y. Ma and D. R. Yang, *J. Phys. Chem. B*, 2006, **110**, 11196-11198.
46. Y. Wang, Q. S. Zhu and H. G. Zhang, *Chem. Commun.*, 2005, 5231-5233.
47. D. B. Kuang, B. X. Lei, Y. P. Pan, X. Y. Yu and C. Y. Su, *J. Phys. Chem. C*, 2009, **113**, 5508-5513.
48. S. Chen, J. W. Zhu, H. Zhou and X. Wang, *RSC Adv.*, 2011, **1**, 484-489.
49. X. A. Chen, X. H. Chen, F. Q. Zhang, Z. Yang and S. M. Huang, *J. Power Sources*, 2013, **243**, 555-561.
50. H. Tüysüz, Y. J. Hwang, S. B. Khan, A. M. Asiri and P. D. Yang, *Nano Res.*, 2012, **6**, 47-54.
51. A. J. Esswein, M. J. McMurdo, P. N. Ross, A. T. Bell and T. D. Tilley, *J. Phys. Chem. C*, 2009, **113**, 15068-15072.
52. I. M. Sadiek, A. M. Mohammad, M. E. El-Shakre and M. S. El-Deab, *Int. J. Hydrogen Energ.*, 2012, **37**, 68-77.

One-step synthesis of multi-walled carbon nanotubes/ultra-thin $Ni(OH)_2$ nanoplate composite as efficient catalysts for water oxidation

Xuemei Zhou,[a] Zhiyun Zhang,[a] Yuanyuan Ma,*[a,b] and Yongquan Qu*[a,b]

[a] *Center for Applied Chemical Research, Frontier Institute of Science and Technology, Xi'an Jiaotong University, Xi'an, 710049, China*

[b] *Institute of Chemistry for New Energy Materials, Department of Chemistry, Xi'an Jiaotong University, Xi'an, China 740049.*

E-mail: yongquan@mail.xjtu.edu.cn; yyma@mail.xjtu.edu.cn

One-step hydrothermal synthesis of ultra-thin β-$Ni(OH)_2$ nanplates (1.5 ~ 3.0 nm thickness) and their composite with multi-walled carbon nanotubes in the absence of surfactants functions as highly efficient and stable electrocatalysts for oxygen evolution reaction.